Macrocyclic effect upon site-selective Cu^{II}M^{II} or M^{II}Cu^{II} core formation with unsymmetric phenol-based macrocyclic ligands†

Masami Yonemura, Naoki Usuki, Yuuki Nakamura, Masaaki Ohba and Hisashi Ōkawa *

Department of Chemistry, Faculty of Science, Kyushu University, Hakozaki, Higashiku 6-10-1, Fukuoka 812-8581, Japan

Complexes of phenol-based dinucleating macrocycles, (L$^{2;2}$)$^{2-}$ and (L$^{2;4}$)$^{2-}$, comprised of two 4-bromo-2-iminomethyl-6-methylaminomethylphenolate moieties combined by an ethylene chain at the amino nitrogens and by an ethylene or a 1,4-tetramethylene chain at the imino nitrogens, have been prepared: mononuclear [Cu(L$^{2;2}$)] and [Cu(L$^{2;4}$)], and dinuclear [PbCu(L$^{2;2}$)][ClO$_4$]$_2$ and [PbCu(L$^{2;4}$)][ClO$_4$]$_2$. The reaction of [Cu(L$^{2;2}$)] and [Cu(L$^{2;4}$)] with MCl$_2$ salts formed dinuclear [MCu(L$^{2;2}$)Cl$_2$] and [MCu(L$^{2;4}$)Cl$_2$] (M = Mn, Co, Ni, Cu or Zn), respectively. A crystallographic study of [NiCu(L$^{2;2}$)Cl$_2$] indicates the Ni^{II} to reside in the aminic site and the Cu^{II} in the iminic site. The complexes, except for that of M = Zn^{II}, show a significant antiferromagnetic interaction within each dinuclear unit. The reaction of [PbCu(L$^{2;2}$)][ClO$_4$]$_2$ with MSO$_4$ salts formed dinuclear Cu^{II}M^{II} perchlorate complexes [CuM(L$^{2;2}$)]-[ClO$_4$]$_2$ (M = Co, Ni, Cu or Zn). A similar transmetallation for [PbCu(L$^{2;4}$)][ClO$_4$]$_2$ caused a scrambling of the metal ions. A crystallographic study of [CuNi(L$^{2;4}$)(dmf)][ClO$_4$]$_2$·MeOH indicates that the Cu^{II} migrates from the iminic to the aminic site to accommodate the Ni^{II} in the iminic site. Kinetic and thermodynamic effects of the macrocycles upon the site selectivity for the metal ions are discussed.

Introduction

Recently, the study of heterodinuclear metal complexes has become important because of unprecedented physicochemical properties and functions arising from a pair of dissimilar metal ions in close proximity.[1–7] In order to provide discrete heterodinuclear core complexes, many efforts have been devoted to the design of unsymmetric compartmental ligands whose two metal-binding sites are not equivalent with respect to the cavity size, co-ordination mode, or the nature of the donor atoms.[8–10] Macrocyclic compartmental ligands have a great advantage over acyclic ligands for this purpose because macrocyclic heterodinuclear cores can be thermodynamically stabilized and kinetically retarded toward metal dissociation and substitution by the so-called 'macrocyclic effect'.[11]

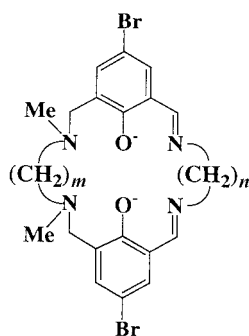The unsymmetric phenol-based macrocycles in Chart 1,

Chart 1 Chemical structure of (L$^{m; n}$)$^{2-}$.

having two dissimilar N(amine)$_2$O$_2$ and N(imine)$_2$O$_2$ metal-binding sites sharing the bridging phenolic oxygens, have been developed in this laboratory;[12–14] they are abbreviated as (L$^{m;n}$)$^{2-}$ using the methylene number (*m*) of the lateral chain combining the amine nitrogens and that (*n*) of the chain combining the imine nitrogens. Previously, we reported a facile synthesis of (L$^{2;3}$)$^{2-}$ as a mononuclear copper(II) complex [Cu(L$^{2;3}$)] and a dinuclear Pb^{II}Cu^{II} complex [PbCu(L$^{2;3}$)][ClO$_4$]$_2$;[12,13] in the formulation [M$_a$M$_b$(L$^{m;n}$)]$^{2+}$, M$_a$ means the metal existing in the aminic site and M$_b$ that in the iminic site. Both the mononuclear and dinuclear complexes can be used as precursors for heterodinuclear M^{II}Cu^{II} or Cu^{II}M^{II} complexes. The mononuclear precursor has the Cu^{II} in the iminic site and can accommodate a second metal(II) ion in the vacant aminic site to form the heterodinuclear M^{II}Cu^{II} chloride complexes [MCu(L$^{2;3}$)Cl$_2$] (M = Mn, Co, Ni or Zn).[14] The transmetallation of Pb^{II} of the Pb^{II}Cu^{II} precursor for a M^{II} was successfully performed by reaction with a metal(II) sulfate salt in an appropriate solvent. The Cu was found to migrate from the iminic site to the aminic site in the transmetallation process providing the Cu^{II}M^{II} perchlorate complexes [CuM(L$^{2;3}$)]-[ClO$_4$]$_2$ (M = Co, Ni or Zn).[13] A similar migration was observed in the conversion of the Pb^{II}Cu^{II} complex into a Zn^{II}Cu^{II} acetate perchlorate complex, [ZnCu(L$^{2;3}$)(AcO)]ClO$_4$. Thus, (L$^{2;3}$)$^{2-}$ shows different site selectivity for metal ions depending upon the synthetic procedure and the counter anion used.

It is naturally expected that the site selectivity for metal ions varies with (L$^{m;n}$)$^{2-}$ ligands. In this study we aim to examine the site selectivity of (L$^{2;2}$)$^{2-}$ and (L$^{2;4}$)$^{2-}$ for metal ions, in comparison with (L$^{2;3}$)$^{2-}$ studied previously. Mononuclear [Cu(L$^{2;2}$)] and [Cu(L$^{2;4}$)] were prepared and their complexation behavior toward metal(II) chlorides was investigated. Further, dinuclear [PbCu(L$^{2;2}$)][ClO$_4$]$_2$ and [PbCu(L$^{2;4}$)][ClO$_4$]$_2$ were prepared, and the transmetallation of Pb^{II} for transition metal(II) ions was studied. Our main focus was placed on kinetic and thermodynamic macrocyclic effects upon site-selective formation of Cu^{II}M^{II} or M^{II}Cu^{II} complexes.

Experimental

Physical measurements

Elemental analyses of C, H, and N were obtained at The Service Center for Elemental Analysis of Kyushu University.

DOI: 10.1039/b006605m

Metal analyses were done on a Shimadzu AA-680 Atomic Absorption/Flame Emission Spectrophotometer. Infrared spectra were recorded on a JASCO IR-810 Spectrophotometer using KBr discs, electronic absorption spectra on a Shimadzu UV-3100PC spectrophotometer and reflectance spectra on a Shimadzu MPS-2000 Spectrophotometer. Molar conductances were measured with a DKK AOL-10 Conductivity Meter at room temperature. Magnetic susceptibilities of powdered samples were measured on a Quantum Design MPMS XL SQUID susceptometer over the temperature range 2–300 K; the apparatus was calibrated with $[Ni(en)_3][S_2O_3]$ (en = ethylenediamine).[15] Effective magnetic moments were calculated by the equation $\mu_{eff} = 2.828(\chi_a T)^{1/2}$ or $2.828(\chi_m T)^{1/2}$, where χ_a and χ_m are the molar magnetic susceptibility per one metal and per molecule, respectively. Diamagnetic corrections for the constituent atoms were done using Pascal's constants.[16] Fast atom bombardment (FAB) mass spectra were recorded on a JMS-SX/SX102A Tandem mass spectrometer using *m*-nitrobenzyl alcohol as a matrix.

Materials

Unless otherwise stated, reagents were purchased from commercial sources and used without further purification. Solvents were dried by standard methods. The synthesis of the proligand *N,N′*-dimethyl-*N,N′*-ethylenedi(5-bromo-3-formyl-2-hydroxybenzylamine) ($H_2L′$) and its mononuclear copper(II) complex $[Cu(L′)]$ were described previously.[12]

Preparations

Precursor complexes. *[Cu(L$^{2;2}$)]·0.5H$_2$O.* To a hot suspension of $[Cu(L′)]$ (0.52 g, 0.9 mmol) in methanol (30 cm³) was added a methanol solution (20 cm³) of ethylenediamine (0.05 g, 0.9 mmol), and the mixture heated for two hours to give a dark brown precipitate. It was collected, washed with diethyl ether and dried *in vacuo*. Yield: 0.40 g (73%). Found: C, 43.67; H, 4.01; Cu, 9.92; N, 9.17%. Calc. for $C_{22}H_{25}Br_2CuN_4O_{2.5}$: C, 43.40; H, 4.14; Cu, 10.44; N, 9.20%. FAB-MS: *m/z* 600 $\{Cu(L^{2;2}) + H\}^+$. UV-Vis in chloroform [λ_{max}/nm (ε/M^{-1} cm^{-1})]: 386 (11040) and 560 (450).

[Cu(L$^{2;4}$)]·H$_2$O. This was obtained as a dark green powder in a way similar to that for $[Cu(L^{2;2})]$ using 1,4-tetramethylenediamine instead of ethylenediamine. Yield: 1.35 g (74%). Found: C, 44.39; H, 4.41; Cu, 9.86; N, 8.51%. Calc. for $C_{24}H_{30}Br_2CuN_4O_3$: C, 44.63; H, 4.68; Cu, 9.84; N, 8.67%. FAB-MS: *m/z* 628 $\{Cu(L^{2;4}) + H\}^+$. UV-Vis in chloroform [λ_{max}/nm (ε/M^{-1} cm^{-1})]: 393 (10600) and 655 (194).

The filtrate was slowly evaporated to form $[Cu(L^{2;4})]·2Me-OH·H_2O$ as green crystals suitable for X-ray crystallography.

[PbCu(L$^{2;2}$)](ClO$_4$)$_2$·0.5H$_2$O. To a hot suspension of $[Cu(L′)]$ (0.58 g, 1 mmol) in chloroform–methanol (15:85 in volume, 30 cm³) was added a methanol solution of lead(II) perchlorate trihydrate (0.46 g, 1 mmol). To the resulting green solution was added dropwise a methanol solution (10 cm³) of ethylenediamine (0.06 g, 1 mmol) to give a dark green powder. Yield: 0.55 g (54%). Found: C, 25.94; H, 2.45; Cu, 6.54; N, 5.24%. Calc. for $C_{22}H_{25}Br_2Cl_2CuN_4O_{10.5}Pb$: C, 26.04; H, 2.48; Cu, 6.26; N, 5.52%. UV-Vis in DMSO [λ_{max}/nm (ε/M^{-1} cm^{-1})]: 366 (8200) and 581 (126).

[PbCu(L$^{2;4}$)](ClO$_4$)$_2$·2H$_2$O. This was obtained as a dark green powder in a way similar to that for $[PbCu(L^{2;2})][ClO_4]_2$ using 1,4-tetramethylenediamine. Yield: 1.59 g (85%). Found: C, 27.01; H, 2.73; Cu, 5.93; N, 5.11%. Calc. for $C_{24}H_{32}Br_2Cl_2CuN_4O_{12}Pb$: C, 26.99; H, 3.02; Cu, 5.90; N, 5.25%. UV-Vis in DMSO [λ_{max}/nm (ε/M^{-1} cm^{-1})]: 358 (8960) and 644 (128).

M^{II}Cu^{II} Chloride complexes (M = Mn, Co, Ni, Cu or Zn). To a hot suspension of $[Cu(L^{m;n})]·nH_2O$ ((*m;n*) = (2;2), (2;4); 0.4 mmol) in methanol (20 cm³) was added a methanol solution (10 cm³) of a metal(II) chloride in a hydrated form (0.4 mmol), and

the green mixture was heated at 50 °C for two hours. The resulting precipitate was isolated by filtration, washed with diethyl ether and dried *in vacuo*.

[MnCu(L$^{2;2}$)Cl$_2$]·0.5H$_2$O 1. Green powder. Yield: 47%. Found: C, 35.77; H, 3.31; Cu, 8.51; Mn, 7.87; N, 7.55%. Calc. for $C_{22}H_{25}Br_2Cl_2CuMnN_4O_{2.5}$: C, 35.97; H, 3.43; Cu, 8.65; Mn, 7.48; N, 7.63%. FAB-MS: *m/z* 689 for $\{MnCu(L^{2;2})Cl\}^+$. UV-Vis on a powdered sample [λ_{max}/nm]: 364, 430 and 645.

[CoCu(L$^{2;2}$)Cl$_2$]·0.5H$_2$O 2. Green crystalline powder. Yield: 79%. Found: C, 35.90; H, 3.30; Co, 7.84; Cu, 8.25; N, 7.59%. Calc. for $C_{22}H_{25}Br_2Cl_2CoCuN_4O_{2.5}$: C, 35.77; H, 3.41; Co, 7.98; Cu, 8.60; N, 7.59%. FAB-MS: *m/z* 693 for $\{CoCu(L^{2;2})Cl\}^+$. UV-Vis on a powderd sample [λ_{max}/nm]: 360, 440 and 650.

[NiCu(L$^{2;2}$)Cl$_2$]·0.5H$_2$O 3. Green crystalline powder. Yield: 41%. Found: C, 35.63; H, 3.32; Cu, 9.12; N, 7.48; Ni, 7.64%. Calc. for $C_{22}H_{25}Br_2Cl_2CuN_4NiO_{2.5}$: C, 35.79; H, 3.41; Cu, 8.61; N, 7.59; Ni, 7.95%. FAB-MS: *m/z* 694 for $\{NiCu(L^{2;2})Cl\}^+$. UV-Vis on a powdered sample [λ_{max}/nm]: 364, 430 and 680.

Single crystals of $[NiCu(L^{2;2})Cl_2]$ **3′** were obtained by diffusing a methanol solution (10 cm³) of nickel(II) chloride hexahydrate (0.5 mmol) into a chloroform solution (20 cm³) of $[Cu(L^{2;2})]·0.5H_2O$ (0.5 mmol).

[Cu$_2$(L$^{2;2}$)Cl$_2$]·0.5H$_2$O 4. Light green crystalline powder. Yield: 76%. Found: C, 35.84; H, 3.35; Cu, 16.51; N, 7.46%. Calc. for $C_{22}H_{25}Br_2Cl_2Cu_2N_4O_{2.5}$: C, 35.55; H, 3.39; Cu, 17.10; N, 7.54%. FAB-MS *m/z*: 699 for $\{CuCu(L^{2;2})Cl\}^+$. UV-Vis on a powdered sample [λ_{max}/nm]: 352, 450 and 720.

[ZnCu(L$^{2;2}$)Cl$_2$]·0.5H$_2$O 5. Bluish green crystalline powder. Yield: 79%. Found: C, 35.64; H, 3.33; Cu, 7.86; N, 7.46; Zn, 8.21%. Calc. for $C_{22}H_{25}Br_2Cl_2CuN_4O_{2.5}Zn$: C, 35.46; H, 3.38; Cu, 8.53; N, 7.52; Zn, 8.78%. FAB-MS: *m/z* 700 for $\{ZnCu(L^{2;2})Cl\}^+$. UV-Vis on a powdered sample [λ_{max}/nm]: 360, 440 and 640.

[MnCu(L$^{2;4}$)Cl$_2$] 6. Brown powder. Yield: 72%. Found: C, 38.09; H, 3.76; Cu, 8.71; Mn, 6.63; N, 7.30%. Calc. for $C_{24}H_{28}Br_2Cl_2CuMnN_4O_2$: C, 38.25; H, 3.74; Cu, 8.43; Mn, 7.29; N, 7.43%. FAB-MS: *m/z* 717 for $\{MnCu(L^{2;4})Cl\}^+$. UV-Vis [λ_{max}/nm (ε/M^{-1} cm^{-1})]: 359 (8550) and 630 (177) in MeOH; 363, 480 and 800 on a powdered sample.

[CoCu(L$^{2;4}$)Cl$_2$]·0.5H$_2$O 7. Green powder. Yield: 70%. Found: C, 37.58; H, 3.75; Co, 7.18; Cu, 8.79; N, 7.25%. Calc. for $C_{24}H_{29}Br_2Cl_2CoCuN_4O_{2.5}$: C, 37.60; H, 3.81; Co, 7.69; Cu, 8.29; N, 7.31%. FAB-MS: *m/z* 721 for $\{CoCu(L^{2;4})Cl\}^+$. UV-Vis [λ_{max}/nm (ε/M^{-1} cm^{-1})]: 354 (8420), 580 (135) and 740 (120) in MeOH; 355, 480, 570 and 800 on a powdered sample.

[NiCu(L$^{2;4}$)Cl$_2$]·0.5H$_2$O 8. Green powder. Yield: 65%. Found: C, 37.50; H, 3.85; Cu, 9.50; N, 7.25; Ni, 6.05%. Calc. for $C_{24}H_{29}Br_2Cl_2CuN_4NiO_{2.5}$: C, 37.61; H, 3.81; Cu, 8.29; N, 7.31; Ni, 7.66%. FAB-MS: *m/z* 722 for $\{NiCu(L^{2;4})Cl\}^+$. UV-Vis [λ_{max}/nm (ε/M^{-1} cm^{-1})]: 352 (9875) and 700 (154) in MeOH; 352, 480 and 800 on a powdered sample.

[Cu$_2$(L$^{2;4}$)Cl$_2$]·0.5H$_2$O 9. Light green powder. Yield: 61%. Found: C, 37.15; H, 3.86; Cu, 15.72; N, 7.11%. Calc. for $C_{24}H_{29}Br_2Cl_2Cu_2N_4O_{2.5}$: C, 37.37; H, 3.79; Cu, 16.48; N, 7.26%. FAB-MS: *m/z* 727 for $\{Cu_2(L^{2;4})Cl\}^+$. UV-Vis [λ_{max}/nm (ε/M^{-1} cm^{-1})]: 349 (9910) and 700 (200) in MeOH; 349, 450 and 800 on a powdered sample.

[ZnCu(L$^{2;4}$)Cl$_2$]·0.5H$_2$O 10. Light green powder. Yield: 60%. Found: C, 37.27; H, 3.72; Cu, 8.63; N, 7.24; Zn, 7.85%. Calc. for $C_{24}H_{29}Br_2Cl_2CuN_4O_{2.5}Zn$: C, 37.28; H, 3.78; Cu, 8.22; N, 7.25; Zn, 8.46%. FAB-MS: *m/z* 728 for $\{ZnCu(L^{2;4})Cl\}^+$. UV-Vis [λ_{max}/nm (ε/M^{-1} cm^{-1})]: 355 (7500) and 670 (194) in MeOH; 284, 353, 455 and 800 on a powdered sample.

Cu^{II}M^{II} Perchlorate complexes (M = Co, Ni, Cu or Zn). To a suspension of $[PbCu(L^{2;2})][ClO_4]_2$ (0.6 mmol) in dry acetonitrile (30 cm³) was added a dry methanol solution of the metal(II) sulfate in a hydrated form (0.6 mmol) in 1:1 stoichiometry, and the mixture stirred at ambient temperature to result in the

Table 1 Crystallographic data of [Cu(L$^{2;4}$)]·2MeOH·H$_2$O, [NiCu(L$^{2;2}$)Cl$_2$] **3′** and [CuNi(L$^{2;2}$)(dmf)][ClO$_4$]$_2$·MeOH **12**

	[Cu(L$^{2;4}$)]·2MeOH·H$_2$O	3′	12
Formula	C$_{26}$H$_{38}$Br$_2$CuN$_4$O$_5$	C$_{22}$H$_{24}$Br$_2$Cl$_2$CuN$_4$NiO$_2$	C$_{26}$H$_{35}$Br$_2$Cl$_2$CuN$_5$NiO$_{12}$
M	709.96	729.42	962.55
Crystal system	Orthorhombic	Monoclinic	Triclinic
Space group	$Pbca$ (no. 61)	$P2_1/n$ (no. 14)	$P\bar{1}$ (no. 2)
a/Å	23.676(6)	10.839(2)	11.124(3)
b/Å	27.32(1)	10.805(2)	16.144(4)
c/Å	8.951(8)	21.387(6)	11.082(4)
a/°			109.15(2)
β/°		91.09(2)	105.59(3)
γ/°			93.44(3)
V/Å^3	5790(4)	2504.4(7)	1786(1)
Z	8	4	2
μ(Mo-Kα)/cm^{-1}	35.65	50.44	35.79
No. of reflections ($I > 3.00\sigma(I)$)	3398	1774	2390
R	0.053	0.046	0.064
Rw	0.043	0.049	0.067

precipitation of PbSO$_4$. It was removed by filtration and the filtrate evaporated to dryness. The residue was extracted with dry acetonitrile, and the extract filtered once to separate PbSO$_4$. The acetonitrile solution was diffused with diethyl ether to give the desired compound.

[CuCo(L$^{2;2}$)](ClO$_4$)$_2$·dmf **11**. Dark green microcrystals after recrystallization from DMF. Yield: 27%. Found: C, 32.50; H, 3.52; Cu, 5.22; Co, 6.31; N, 7.55%. Calc. for C$_{25}$H$_{31}$Br$_2$Cl$_2$-CoCuN$_5$O$_{11}$: C, 32.26; H, 3.36; Cu, 6.83; Co, 6.33; N, 7.52%. UV-Vis [λ_{max}/nm (ε/M^{-1} cm^{-1})]: 369 (6720) and 650 (150) in DMSO; 361 and 622 (sh) on a powdered sample.

[CuNi(L$^{2;2}$)][ClO$_4$]$_2$·dmf·MeOH **12**. Reddish brown crystals when recrystallized from a dmf–methanol mixture. Yield: 47%. Found: C, 32.21; H, 3.40; Cu, 6.69; Ni, 6.15%. Calc. for C$_{26}$H$_{35}$Br$_2$Cl$_2$CuN$_5$NiO$_{12}$: C, 32.44; H, 3.67; Cu, 6.60; N, 7.28; Ni, 6.10%. UV-Vis [λ_{max}/nm (ε/M^{-1} cm^{-1})]: 324 (10960), 374 (7130), 530 (sh) (310) and 670 (94) in DMSO; 367, 540 (sh) and 648 on a powdered sample.

[Cu$_2$(L$^{2;2}$)][ClO$_4$]$_2$·MeCN **13**. Green powder. Yield: 64%. Found: C, 31.96; H, 3.06; Cu, 14.02; N, 7.74%. Calc. for C$_{24}$-H$_{27}$Br$_2$Cl$_2$Cu$_2$N$_5$O$_{10}$: C, 31.91; H, 3.01; Cu, 14.07; N, 7.75%. UV-Vis [λ_{max}/nm (ε/M^{-1} cm^{-1})]: 351 (9800) and 610 (230) in DMSO; 350 (9320) and 590 (220) in dmf; 350 and 560 (br) on a powdered sample.

*[CuZn(L$^{2;2}$)][ClO$_4$]$_2$·H$_2$O* **14**. Green powder. Yield: 35%. Found: C, 30.17; H, 3.10; Cu, 6.74; N, 6.60; Zn, 7.92%. Calc. for C$_{22}$H$_{26}$Br$_2$Cl$_2$CuN$_4$O$_{11}$Zn: C, 29.95; H, 2.97; Cu, 7.20; N, 6.35; Zn, 7.41%. UV-Vis [λ_{max}/nm (ε/M^{-1} cm^{-1})]: 349 (9600) and 646 (120) in DMSO; 363 and 576 on a powdered sample.

Single crystal X-ray analyses for [Cu(L$^{2;4}$)]·2MeOH·H$_2$O, [NiCu(L$^{2;2}$)Cl$_2$] 3′ and [CuNi(L$^{2;2}$)(DMF)](ClO$_4$)$_2$·MeOH 12

Crystallographic measurements were made on a Rigaku AFC7R diffractometer with graphite monochromated Mo-Kα radiation ($\lambda = 0.71069$ Å) and a 12 kW rotating anode generator. Cell constants and an orientation matrix for the data collection were obtained from 25 reflections and the ω–2θ scan mode was used for the intensity collections at 20 ± 1 °C. The octant measured was $+h$, $+k$, $\pm l$ for all the complexes. Pertinent crystallographic parameters are summarized in Table 1.

Three standard reflections were monitored every 150 measurements. Over the course of data collection the standards decreased by 2.2% for [Cu(L$^{2;4}$)]·2MeOH·H$_2$O, increased by 0.4% for **3′** and decreased by 10.9% for **12**. A linear correction factor was applied. Reflection data were corrected for Lorentz and polarization effects.

The structures were solved by the direct method and expanded using Fourier techniques. The non-hydrogen atoms were refined anisotropically. Hydrogen atoms were included in
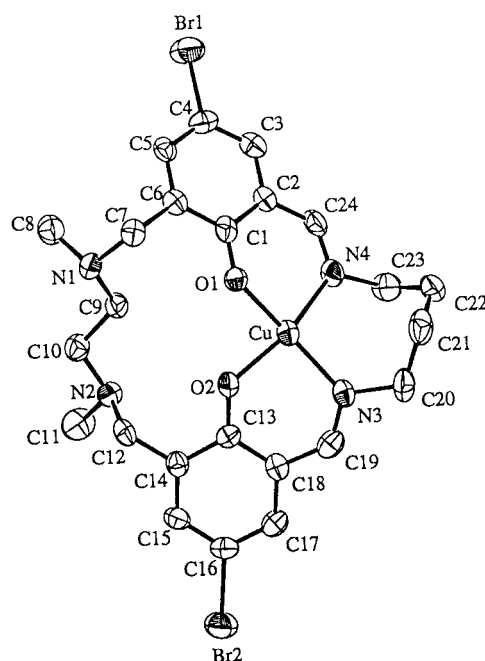
Fig. 1 An ORTEP view of [Cu(L$^{2;4}$)]·2MeOH·H$_2$O with the atom numbering scheme.

the structure factor calculation but not refined. Computations were carried out on an IRIS Indigo computer using the TEXSAN crystallographic software package[17]

CCDC reference number 186/2153.

See http://www.rsc.org.suppdata/dt/b0/b006605m/ for crystallographic files in .cif format.

Results and discussion

Precursor complexes

Preparation. The mononuclear copper(II) complexes [Cu(L$^{2;2}$)] and [Cu(L$^{2;4}$)] were prepared by a template reaction similar to that for [Cu(L$^{2;3}$)].[12] In our preliminary study, the cyclization of [Cu(L′)] with ethylenediamine in a concentrated dmf solution was found to cause the formation of the [2:2] condensation product together with the desired [1:1] condensation product, [Cu(L$^{2;2}$)].[18] In order to avoid contamination of the [2:2] condensation product, the syntheses of [Cu(L$^{2;2}$)] and [Cu(L$^{2;4}$)] were carried out in a rather dilute solution in methanol. FAB mass spectra for the products show a dominant ion peak corresponding to {Cu(L$^{m;n}$)+H}$^+$, indicating no contamination of higher condensation products.

Table 2 Selected bond distances (Å) and angles (°) for [Cu(L$^{2;4}$)]·2MeOH·H$_2$O

Cu(1)–O(1)	1.906(5)	Cu(1)–O(2)	1.908(5)
Cu(1)–N(3)	1.988(6)	Cu(1)–N(4)	1.980(6)
O(1)–Cu(1)–O(2)	85.7(2)	O(1)–Cu(1)–N(3)	159.1(2)
O(1)–Cu(1)–N(4)	91.9(2)	O(2)–Cu(1)–N(3)	92.0(3)
O(2)–Cu(1)–N(4)	152.7(3)	N(3)–Cu(1)–N(4)	99.4(3)

Dihedral angle	
O(1)Cu(1)N(4)–O(2)Cu(1)N(3)	32.48

The dinuclear Pb^{II}Cu^{II} complexes, [PbCu(L$^{2;2}$)][ClO$_4$]$_2$ and [PbCu(L$^{2;4}$)][ClO$_4$]$_2$, were prepared by template cyclization of [Cu(L′)] with ethylenediamine or tetramethylenediamine, respectively, in the presence of Pb^{II} as the template ion.[13]

Crystal structure of [Cu(L$^{2;4}$)]·2MeOH·H$_2$O. An ORTEP[19] view of the essential part of the complex is shown in Fig. 1 together with the numbering scheme. Selected bond distances and angles are given in Table 2. The result clearly demonstrates that the Cu^{II} resides in the iminic site of the macrocycle (L$^{2;4}$)$^{2-}$. The two methanol molecules and one water molecule are free from co-ordination and are captured in the crystal lattice. The Cu has a four-co-ordinate environment with the Cu–O and Cu–N bond distances ranging from 1.906(5) to 1.988(6) Å. The geometry about the Cu shows a tetrahedral distortion; the dihedral angle between the least-squares plane defined by O1, Cu and N4 and the plane defined by O2, Cu and N3 is 32.48°. A slightly larger dihedral angle (35.56°) is found for the analogous [Cu(L$^{2;3}$)].[13]

Properties. The absorption spectra of [Cu(L$^{2;2}$)] and [Cu(L$^{2;4}$)] in chloroform show a superimposed copper d–d band at 560 and 655 nm, respectively, compared to the band maximum of *N,N′*-bis(salicylidene)ethylenediaminatocopper(II) (558 nm in chloroform[20]) and that of *N,N′*-bis(salicylidene)tetramethylenediaminatocopper(II) (649 nm in Nujol mulls[21]), respectively. [Cu(L$^{2;3}$)] shows a corresponding d–d band maximum at 620 nm (in chloroform) compared to that of *N,N′*-bis(salicylidene)trimethylenediaminatocopper(II) (602 in Nujol mull[21] and 605 nm in acetonitrile[22]). Thus, the d–d band maximum shifts to a longer wavelength with elongation of the lateral chain in the iminic site. An intense band around 380 nm is assigned to the π–π* transition band of the azomethine group.[23,24]

[PbCu(L$^{2;2}$)][ClO$_4$]$_2$ and [PbCu(L$^{2;4}$)][ClO$_4$]$_2$ in DMSO show a coper d–d band maximum at 581 and 644 nm, respectively. The azomethine π–π* band for these Pb^{II}Cu^{II} complexes is located at 358–366 nm.

[Cu(L$^{2;2}$)] and [Cu(L$^{2;4}$)] are non-electrolytes in DMSO. The molar conductances of [PbCu(L$^{2;2}$)][ClO$_4$]$_2$ and [PbCu(L$^{2;4}$)]-[ClO$_4$]$_2$ in DMSO (60–61 S cm^2 mol^{-1}) are characteristic of 2:1 electrolytes in this solvent.[25]

M^{II}Cu^{II} chloride complexes

Preparation. Mononuclear [Cu(L$^{2;2}$)] and [Cu(L$^{2;4}$)] have the Cu in the iminic site and can accommodate a second M^{II} ion in the vacant N(amine)$_2$O$_2$ site. The reaction of the complexes with M^{II}Cl$_2$ in methanol formed M^{II}Cu^{II} chloride complexes **1–10** in a good yield (see Scheme 1, top). FAB mass spectra for the heterodinuclear complexes (**1–3**, **5–8** and **10**) showed a dominant molecular ion peak corresponding to the {MCu(L$^{m;n}$)Cl}$^+$ fragment; no ion peak due to homodimetallic Cu^{II}Cu^{II} and M^{II}M^{II} species was detected. Thus, (L$^{2;2}$)$^{2-}$ and (L$^{2;4}$)$^{2-}$ show a site selectivity for metal ions in forming the M^{II}Cu^{II} chloride complexes as found for (L$^{2;3}$)$^{2-}$ previously.[14]

Crystal structure of [NiCu(L$^{2;2}$)Cl$_2$] 3′. An ORTEP view of complex **3′** is shown in Fig. 2 together with the numbering
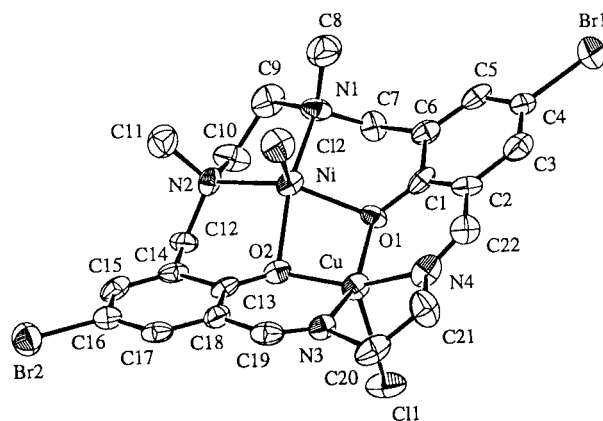
Fig. 2 An ORTEP view of [NiCu(L$^{2;2}$)Cl$_2$] **3′** with the atom numbering scheme.
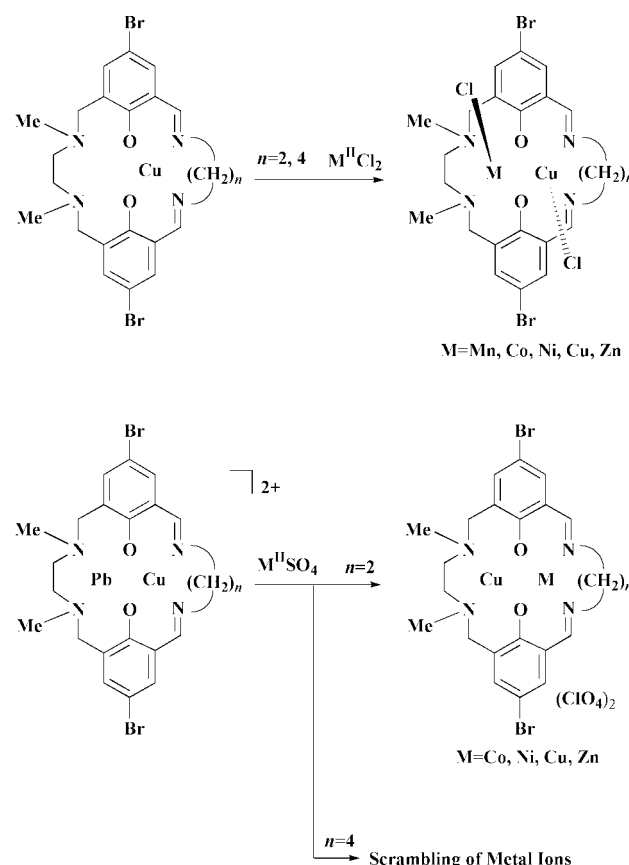
Scheme 1 Synthetic schemes for the M^{II}Cu^{II} chloride and Cu^{II}M^{II} perchlorate complexes.

scheme. Selected bond distances and angles are given in Table 3. The structure analysis demonstrates that the Cu^{II} resides in the original iminic site and the Ni^{II} in the aminic site. The Ni · · · Cu intermetallic separation bridged by the phenolic oxygens is 2.975(2) Å and the Ni–O1–Cu and Ni–O2–Cu angles are 97.9(4) and 97.2(4)°, respectively. Both Cu^{II} and Ni^{II} have a five-co-ordinate geometry including a chloride ion. The configuration about the Cu is best described as square pyramidal with the chloride ion at the apex; the discrimination parameter τ[26] (square pyramid, τ = 0; trigonal bipyramid, τ = 1) is 0.047. The equatorial Cu-to-ligand bond distances range from 1.937(8) to 1.96(1) Å, whereas the axial Cu–Cl bond distance is elongated (2.560(4) Å) due to the Jahn–Teller effect in the d^9 electronic configuration of Cu^{II}. The deviation of Cu from the basal N$_2$O$_2$ least-squares plane toward the axial Cl is 0.406 Å.

Table 3 Selected bond distances (Å) and angles (°) for [NiCu(L²·²)Cl₂] **3′**

Ni–O(1)	2.005(8)	Cu–O(2)	1.937(8)
Ni–O(2)	2.027(8)	Cu–N(3)	1.94(1)
Ni–N(1)	2.06(1)	Cu–N(4)	1.96(1)
Ni–N(2)	2.05(1)	Cu–Cl(1)	2.560(4)
Ni–Cl(2)	2.275(4)	Ni···Cu	2.975(2)
Cu–O(1)	1.940(8)		
Ni–O(1)–Cu	97.9(3)	N(1)–Ni–N(2)	87.4(4)
Ni–O(2)–Cu	97.2(4)	Cl(1)–Cu–O(1)	111.1(3)
Cl(2)–Ni–O(1)	100.7(3)	Cl(1)–Cu–O(2)	100.5(3)
Cl(2)–Ni–O(2)	97.9(3)	Cl(1)–Cu–N(3)	94.3(3)
Cl(2)–Ni–N(1)	104.1(3)	Cl(1)–Cu–N(4)	102.2(3)
Cl(2)–Ni–N(2)	109.9(3)	O(1)–Cu–O(2)	79.7(3)
O(1)–Ni–O(2)	76.1(3)	O(1)–Cu–N(3)	154.5(4)
O(1)–Ni–N(1)	93.8(4)	O(1)–Cu–N(4)	91.5(4)
O(1)–Ni–N(2)	148.1(4)	O(2)–Cu–N(3)	93.5(4)
O(2)–Ni–N(1)	157.2(4)	O(2)–Cu–N(4)	157.3(4)
O(2)–Ni–N(2)	90.6(4)	N(3)–Cu–N(4)	85.5(4)

Dihedral angle	
O(1)O(2)N(1)N(2)–O(1)O(2)N(3)N(4)	28.43

Fig. 3 $\chi_m T$ *vs.* T plots for complexes **1**–**3** and χ_a *vs.* T plot for **4**.

The geometry about the Ni^{II} is also square pyramidal with the chloride ion at the apex; τ is 0.153. The Ni is displaced 0.471 Å from the basal N₂O₂ least-squares plane towards the axial Cl. This is considerably large compared with that of [NiCu(L²·³)Cl₂] reported previously.[13] The basal Ni-to-ligand bond distances range from 2.005(8) to 2.06(1) Å and the axial Ni–Cl bond distance is 2.275(4) Å.

The chloride ligand at the axial site of the Cu and that at the axial site of the Ni are situated *trans* to each other with respect to the mean molecular plane. The dihedral angle between the basal N(amine)₂O₂ and N(imine)₂O₂ least-squares planes is 28.43°. The asymmetric nitrogens N1 and N2 have *S* and *R* configuration, respectively. The two methyl substituents attached to the amino nitrogens are situated *cis* to each other, and the Cu is displaced to the *N*-methyl substituent side. Thus, the *N*-methyl groups and the chloride ion attached to the Ni^{II} are arranged *cis* to each other.

Properties. Complexes **1**–**5** were sparingly soluble in common organic solvents. Therefore, their electronic spectra were measured by reflection on powdered samples. They show a band maximum around 640–720 nm that can be assigned to the superposed d–d band of the Cu^{II}. The copper band maximum for **1**–**5** is located at a longer wavelength than that of 576 nm for [Cu(L²·²)], in accord with the axial co-ordination of chloride ion. A discernible shoulder is seen around 440 nm which is ascribed to charge transfer from Cl⁻ to Cu^{II}. The azomethine π–π* transition band is observed near 360 nm.

The electronic spectra of complexes **6**–**10** were measured by reflection on powdered samples and by absorption in methanol. They show the copper(II) d–d band maximum around 800 nm on powdered samples whereas at 630–740 nm in methanol. The reflectance spectra show a shoulder at 450–480 nm attributable to charge transfer from Cl⁻ to Cu^{II}. The CT band disappears in methanol. The molar conductances of **6**–**10** in methanol (57–86 S cm² mol⁻¹) are characteristic of 1:1 electrolytes in this solvent. Evidently, the chloride ion bonded to the axial site of the Cu^{II} is dissociated in methanol.

The Zn^{II}Cu^{II} complexes **5** and **10** have magnetic moments indicating one unpaired electron (1.85 and 1.89 μ_B, respectively). The other complexes show a subnormal magnetic moment at room temperature, suggesting an antiferromagnetic spin-exchange interaction within each dinuclear unit. The $\chi_m T$ *vs.* T plots for **1**–**3** are given in Fig. 3. The χ_a *vs.* T plot for **4** is given as an insert in Fig. 3.

The $\chi_m T$ value for complex **1** (MnCu) at 300 K is 4.26 cm³ K mol⁻¹ (5.84 μ_B) which decreased with decreasing temperature
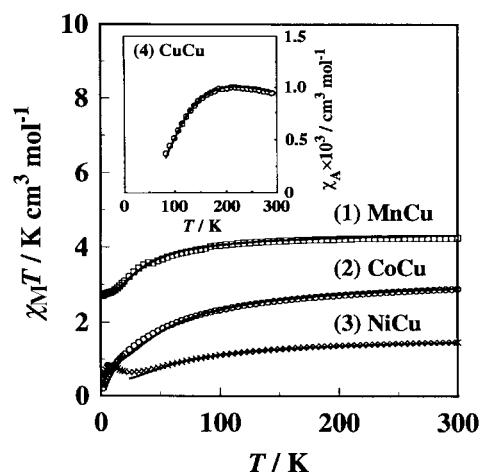
to 2.72 cm³ K mol⁻¹ (4.66 μ_B) at 2 K. A magnetic analysis has been made using the magnetic susceptibility expression (1) for

$$\chi_m = \{(N\beta^2/kT)[28g_3^2 + 10g_2^2\exp(-6J/kT)]/ \\ [7 + 5\exp(-6J/kT)]\} + N_\alpha \quad (1)$$

the $(S_{Cu} = 1/2)$–$(S_{Mn} = 5/2)$ system based on the isotropic Heisenberg model $(H = -2JS_{Cu}S_{Mn})$,[13] where N is Avogadro's number, β the Bohr magneton, k the Boltzmann constant, J the exchange integral, T the absolute temperature, N_α the temperature-independent paramagnetism, and g_2 and g_3 are g factors associated with the total spin states $S_T = 2$ and 3, respectively. The g factors were expressed using the local g_{Mn} and g_{Cu} values as follows:[27,28] $g_2 = (7g_{Mn} - g_{Cu})/6$ and $g_3 = (5g_{Mn} + g_{Cu})/6$. In magnetic simulations g_{Mn} and N_α were fixed at 2.00 and 60×10^{-6} cm³ mol⁻¹, respectively. A good simulation was obtained as indicated by the solid line in Fig. 3 using $J = -6.0$ cm⁻¹ and $g_{Cu} = 2.05$.

The $\chi_m T$ value for complex **2** (CoCu) at 300 K is 2.89 cm³ K mol⁻¹ (4.81 μ_B) wich decreased with decreasing temperature to 0.21 cm³ K mol⁻¹ (1.30 μ_B) at 2 K. The moment at 2.0 K is lower than the spin-only value for $S_T = 1$ arising from spin coupling between Cu^{II} ($S = 1/2$) and Co^{II} ($S = 3/2$). This fact means the operation of secondary contribution(s) such as the orbital effect of the $^4T_{2g}$ ground term and/or zero-field splitting of Co^{II}. The magnetic susceptibility for the $(S_{Co} = 3/2)$–$(S_{Cu} = 1/2)$ system is given by eqn. (2), where θ is the correction term for the

$$\chi_m = \{[N\beta^2/k(T - \theta)][10g_2^2 + 2g_1^2\exp(-4J/kT)]/ \\ [5 + 3\exp(-4J/kT)]\} + N_\alpha \quad (2)$$

secondary contribution(s) and g_1 and g_2 are g factors associated with the total spin states $S_T = 1$ and 2, respectively. The g factors were expressed using the local g_{Co} and g_{Cu} values as follows:[27,28] $g_1 = (5g_{Co} - g_{Cu})/4$ and $g_2 = (3g_{Co} + g_{Cu})/4$. Owing to the large secondary contribution, cryomagnetic simulations for **2** were carried out using fixed $g_{Co} = 2.3$, $g_{Cu} = 2.1$ and $N_\alpha = 300 \times 10^{-6}$ cm³ mol⁻¹ to obtain $J = -15$ cm⁻¹ and $\theta = -6$ K.

The $\chi_m T$ value for complex **3** (NiCu) at room temperature is 1.46 cm³ K mol⁻¹ (= 3.46 μ_B) which decreased with decreasing temperature to a minimum of 0.65 cm³ K mol⁻¹ (2.27 μ_B) around 24 K, increasing to 0.84 cm³ K mol⁻¹ (2.59 μ_B) at 8 K, and then decreasing to 0.53 cm³ K mol⁻¹ (2.06 μ_B) at 2 K. The unusual magnetic behavior in the low temperature region was observed in measurements for different samples. The magnetic susceptibility for the $(S_{Ni} = 1)$–$(S_{Cu} = 1/2)$ system is given by eqn. (3), where $g_{1/2}$ and $g_{3/2}$ indicate the g factors associated with

$$\chi_m = \{(N\beta^2/4kT)[10g_{3/2}^2 + g_{1/2}^2\exp(-3J/kT)]/ \\ [2 + \exp(-3J/kT)]\} + N_\alpha \quad (3)$$

the total spin states $S_T = 1/2$ and $3/2$, respectively. The g values were expressed using local g factors as $g_{1/2} = (4g_{Ni} - g_{Cu})/3$ and $g_{3/2} = (2g_{Ni} + g_{Cu})/3$. Magnetic simulations for **3** were carried out in the range 50–300 K, using fixed $g_{Ni} = 2.10$, $g_{Cu} = 2.05$ and $N_\alpha = 280 \times 10^{-6}$ cm^3 mol^{-1}, to obtain $J = -24$ cm^{-1}. The unusual magnetic behavior at low temperature remains to be studied further.

Magnetic analyses for complex **4** (Cu$_2$) have been done using the Bleaney–Bowers equation[33] (4). A good fit was obtained

$$\chi_a = \{Ng^2\beta^2/kT\}[\exp(-2J/kT) + 3]^{-1} + N_\alpha \quad (4)$$

with $-J = 122$ cm^{-1} when simulated with fixed $g = 2.10$ and $N_\alpha = 60 \times 10^{-6}$ cm^3 mol^{-1}.

The magnetic moments of complexes **6**, **7**, **8** and **9** at room temperature are 5.66, 4.63, 3.06 and 1.18 μ_B, respectively. Cryomagnetic measurements for **6**, **8** and **9** suggested contamination by paramagnetic impurity in each sample. In the first approximation the paramagnetic impurity was supposed to be a monomeric copper(II) species, and magnetic analyses were carried out by the modified eqns. (1′), (3′) and (4′) including a

$$\chi_m = \{(1 - \rho)(N\beta^2/kT)[28g_3^2 + 10g_2^2\exp(-6J/kT)]/ \\ [7 + 5\exp(-6J/kT)]\} + \rho(N\beta^2/kT) + N_\alpha \quad (1')$$

$$\chi_m = \{(1 - \rho)\{N\beta^2/4kT)[10g_{3/2}^2 + g_{1/2}^2\exp(-3J/kT)]/ \\ [2 + \exp(-3J/kT)]\} + \rho(N\beta^2/kT) + N_\alpha \quad (3')$$

$$\chi_a = (1 - \rho)\{Ng^2\beta^2/kT\}[\exp(-2J/kT) + 3]^{-1} + \\ \rho(N\beta^2/kT) + N_\alpha \quad (4')$$

correction term for the monomeric species. In these equations ρ means the fraction of the impurity. The following best-fit parameters were obtained: $J = -15$ cm^{-1}, $g_{Cu} = 2.02$, $g_{Mn} = 2.0$, $N_\alpha = 60 \times 10^{-6}$ cm^3 mol^{-1} and $\rho = 0.15$ for **6**; $J = -19$ cm^{-1}, $g_{Cu} = 2.05$, $g_{Co} = 2.15$, $\theta = -7$ K and $N_\alpha = 300 \times 10^{-6}$ cm^3 mol^{-1} for **7**; $J = -55$ cm^{-1}, $g_{Cu} = 2.03$, $g_{Ni} = 2.10$, $N_\alpha = 280 \times 10^{-6}$ cm^3 mol^{-1} and $\rho = 0.12$ for **8**; $J = -210$ cm^{-1}, $g = 2.10$, $N_\alpha = 60 \times 10^{-6}$ cm^3 mol^{-1} and $\rho = 0.02$ for **9** (see ESI Supplementary Material). Such a large ρ value for **6** and **8** is unlikely judged from the good analytical data for these complexes. We presume the paramagnetic impurity in **6** and **8** to be a monomeric manganese(II) and a monomeric nickel(II) species, respectively. Based on this presumption, the impurity fraction for **6** and **8** is evaluated to be 0.013 and 0.045, respectively.

## Cu^{II}M^{II} Perchlorate complexes

Preparation. The transmetallation of Pb^{II} of [PbCu(L$^{2;2}$)]-[ClO$_4$]$_2$ for a metal(II) ion could successfully be performed by treating the PbCu complex with a metal(II) sulfate salt, providing Cu^{II}M^{II} perchlorate complexes (M = Co **11**, Ni **12** or Zn **14**) (Scheme 1, bottom). A similar transmetallation using manganese(II) sulfate tetrahydrate resulted in a scrambling of metal ions to give [Cu$_2$(L$^{2;2}$)][ClO$_4$]$_2$ **13** as the main product. Such a scrambling also occurred in the transmetallation of [PbCu(L$^{2;4}$)][ClO$_4$]$_2$. Thus, (L$^{2;2}$)$^{2-}$ shows a site selectivity of metal ions to form the Cu^{II}M^{II} perchlorate complexes, as observed for (L$^{2;3}$)$^{2-}$ previously,[13] but not for (L$^{2;4}$)$^{2-}$.

Crystal structure of [CuNi(L$^{2;2}$)(dmf)][ClO$_4$]$_2$·MeOH 12. An ORTEP view of the cationic part of complex **12** is shown in Fig. 4 together with the numbering scheme. Selected bond distances and angles are given in Table 4. The crystallography clearly demonstrates that the Cu migrates from the iminic site to aminic site and the Ni is accommodated in the iminic site. The cation is comprised of (L$^{2;2}$)$^{2-}$, one Cu^{II}, one Ni^{II}, and one dmf molecule; two perchlorate ions and a methanol molecule are free from co-ordination and captured in the crystal lattice. The Cu$\cdots$Ni intermetallic separation bridged by the phenolic

Table 4 Selected bond distances (Å) and angles (°) for [CuNi(L$^{2;2}$)-(dmf)][ClO$_4$]$_2$·MeOH **12**

Cu–O(1)	1.960(9)	Ni–O(1)	1.861(9)
Cu–O(2)	1.961(9)	Ni–O(2)	1.84(1)
Cu–O(3)	2.20(1)	Ni–N(3)	1.85(1)
Cu–N(1)	1.98(1)	Ni–N(4)	1.82(1)
Cu–N(2)	2.00(1)	Cu$\cdots$Ni	2.836(3)
Cu–O(1)–Ni	95.8(5)	O(3)–Cu–N(1)	105.8(5)
Cu–O(2)–Ni	96.3(5)	O(3)–Cu–N(2)	107.9(5)
O(1)–Cu–O(2)	75.1(4)	N(1)–Cu–N(2)	90.4(5)
O(1)–Cu–O(3)	87.2(4)	O(1)–Ni–O(2)	80.3(4)
O(1)–Cu–N(1)	94.8(4)	O(1)–Ni–N(3)	175.0(6)
O(1)–Cu–N(2)	162.1(4)	O(1)–Ni–N(4)	96.6(5)
O(2)–Cu–O(3)	93.1(4)	O(2)–Ni–N(3)	94.9(6)
O(2)–Cu–N(1)	158.2(4)	O(2)–Ni–N(4)	176.5(5)
O(2)–Cu–N(2)	94.0(5)	N(3)–Ni–N(4)	88.2(6)

Dihedral angles

O(1)O(2)N(1)N(2)–O(1)O(2)N(3)N(4)   23.92
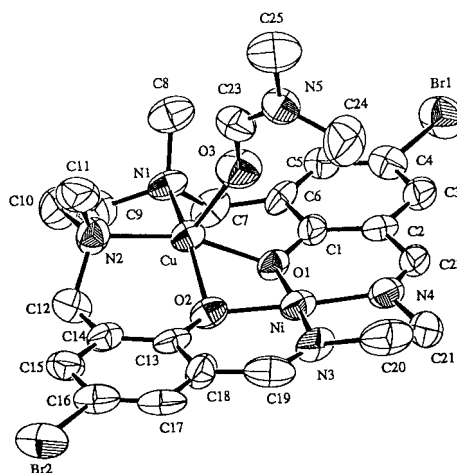
Fig. 4 An ORTEP view of [CuNi(L$^{2;2}$)(dmf)][ClO$_4$]$_2$·MeOH **12** with the atom numbering scheme.

oxygens is 2.836(3) Å. The Cu–O1–Ni and Cu–O2–Ni angles are 95.8(5) and 96.3(5)°, respectively.

The Cu has a square-pyramidal geometry with a dmf oxygen at the apex; τ is 0.07. The equatorial Cu-to-ligand bond distances fall in the range 1.960(9)–2.00(1) Å. The axial Cu–O(dmf) bond distance is elongated (2.20(1) Å) due to the Jahn–Teller effect. The deviation of the Cu^{II} from the basal N$_2$O$_2$ least-squares plane toward the axial O(dmf) atom is 0.313 Å. The geometry about the Ni is square planar and resembles that of [Ni(salen)].[30] The equatorial Ni-to-ligand bond distances fall in the range 1.82(1)–1.86(1) Å.

The asymmetric amino nitrogens N1 and N2 have S and R configuration, respectively; the two methyl groups attached to the amino nitrogens are situated *cis* to each other. The Cu is displaced to the methyl substituent side. Thus, the dmf molecule bonded to the axial site of the Cu and the N-methyl groups are arranged *cis* to each other. The dihedral angle between the N(amine)$_2$O$_2$ and N(imine)$_2$O$_2$ least-squares planes at the O1$\cdots$O2 edge is 23.92°.

Properties. The molar conductances of complexes **11**–**14** in DMSO fall in the range of 66–80 S cm^2 mol^{-1} characteristic of 2 : 1 electrolytes in this solvent. The electronic spectra in DMSO showed a superposed copper d–d band around 610–670 nm compared to the d–d band for analogous complexes of (L$^{2;3}$)$^{2-}$ ($\approx$ 630 nm). Complex **12** (CuNi) shows an additional band around 530 nm assigned to a d–d component of the low-spin Ni^{II} in the 'salen'-like iminic site.[31,32] It should be mentioned that the CuNi perchlorate complex of (L$^{2;3}$)$^{2-}$ shows a d–d component of high-spin Ni^{II} near $\approx$ 750 nm.

The magnetic properties of complexes **11–14** were studied in the temperature range 80–290 K. Complex **14** (CuZn) shows a magnetic moment for one unpaired electron (1.85 μ_B). The room-temperature magnetic moment of **11** is 3.22 μ_B (per CuCo) that is significantly small compared with the moments of the $Cu^{II}Co^{II}$(high-spin) chloride complexes **2** (4.81 μ_B) and **7** (4.63 μ_B). When the magnetic moments for Cu^{II} and low-spin Co^{II} are assumed to be 1.85 and 1.9–2.7 μ_B,[33] respectively, a magnetic moment of 2.65–3.27 μ_B is expected for the magnetically non-interacting $Cu^{II}(S = 1/2)$–$Co^{II}(S = 1/2)$ system. That of **11** falls in this range. This fact means that the Co resides in the iminic site and assumes a low-spin state ($S_{Co} = 1/2$) as in the case of [Co(salen)]. The moment decreased with decreasing temperature to 2.81 μ_B near liquid nitrogen temperature, suggesting an antiferromagnetic interaction within the molecule. However, the exchange integral was not evaluated in this work because the magnetic moment of low-spin Co^{II} itself is often dependent upon temperature.[33]

Complex **12** (CuNi) has a magnetic moment of 1.95 μ_B, independent of temperature down to 80 K. Evidently, the Ni^{II} is diamagnetic in accord with its planar configuration.

Complex **13** (Cu$_2$) has a subnormal magnetic moment (1.35 μ_B per Cu) and shows a temperature dependence of magnetic moment typical of antiferromagnetic interaction. Magnetic analyses were made based on the Bleaney–Bowers eqn. (4), giving the best-fit parameters $J = -130$ cm^{-1}, $g = 2.00$, $\rho = 0.02$ and $N_\alpha = 60 \times 10^{-6}$ cm^3 mol^{-1}.

Site selectivity of metal ions

It is evident that the macrocycles $(L^{2;2})^{2-}$, $(L^{2;3})^{2-}$ and $(L^{2;4})^{2-}$ show a site selectivity for metal ions, along with exogenous chloride ion, forming $M^{II}Cu^{II}$ chloride complexes having the M^{II} in the aminic site and the Cu^{II} in the iminic site. This site selectivity naturally arises from the 'thermodynamic effect' of the macrocycles providing a specific stability for a heterodinuclear core with its two dissimilar metal-binding sites. The chloride ligation to the M^{II} in the aminic site is important for stabilizing the heterodinuclear $M^{II}Cu^{II}$ core; the chloride ligation to the Cu^{II} is not significant for the site selectivity because the chloride is dissociated in methanol for the complexes of $(L^{2;4})^{2-}$. The two methyl groups attached to the amine nitrogens are situated *cis* with respect to the mean N(amine)$_2$O$_2$ plane which gives rise to a specific geometric requirement for the metal at the aminic site. That is, the preferred geometry about the M^{II} is a square pyramidal with a large displacement of the metal from the basal plane to the methyl substituent side. Five-co-ordinate Mn^{II}, Co^{II}, Ni^{II} or Zn^{II} with chloride ligation can be accommodated in the aminic site, whereas Cu^{II} prefers the iminic site that can provide a planar environment favorable for this metal ion.

Of particular interest is the copper migration in the transmetallation of the Pb^{II} of $[PbCu(L^{2;2})][ClO_4]_2$ (and $[PbCu(L^{2;3})][ClO_4]_2$[13]) for a metal(II) ion to afford the $Cu^{II}M^{II}$ perchlorate complexes. This site selectivity for metal ions may be kinetically controlled. A mechanistic scheme for the copper migration is considered here. The dissociation of Pb^{II} prior to the attack of M^{II} is unlikely because this may afford $M^{II}Cu^{II}$ complexes. Based on the X-ray crystallography of a $Pb^{II}Cu^{II}$ complex of $(L^{2;3})^{2-}$,[13] the aminic and iminic least-squares planes are bent at the O···O edge with a dihedral angle of 14.87°. This means the bridging phenolic oxygens have a sp^3 hybridization character. Thus, the $Pb^{II}Cu^{II}$ complex can co-ordinate to a metal(II) ion through the phenolic oxygens to form a di(μ_3-phenoxo) $Pb^{II}Cu^{II}M^{II}$ complex (Scheme 2). Two pathways, **A** and **B**, are considered. Pathway **A** involves the approach of M to the iminic site, followed by migration of Cu to the aminic site and release of Pb from the aminic site. This can be performed without cleavage of the O–Cu and O–M bonds, by rotating the O–Cu and O–M linkages about the
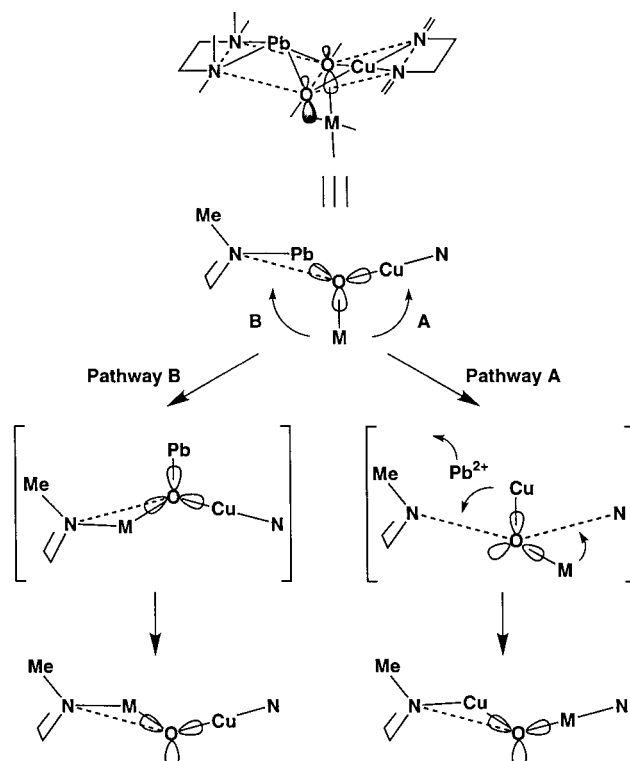
Scheme 2 A mechanistic scheme for the copper migration in transmetallation of [PbCu(L$^{m;n}$)].

O···O axis (see Scheme 2). When M approaches the aminic site to kick out the Pb (pathway **B**), a $M^{II}Cu^{II}$ core may be formed. This is not the case observed in this work. In fact, pathway **B** is ruled out because this necessitates a large molecular change with respect to the bending at the O···O edge and the {MN(amine)$_2$O$_2$} chromophore in this transition state must adopt an unfavorable configuration with the Cu displaced to the ethylene chain side. Thus, pathway **A** can reasonably explain the result observed in this work. A similar copper migration can occur in the transmetallation of $[PbCu(L^{2;4})][ClO_4]_2$, but the resulting $[CuM(L^{2;4})][ClO_4]_2$ must be unstable in the thermodynamic sense, causing a scrambling of metal ions. Detailed kinetic studies for the transmetallation are underway.

In conclusion, studies on heterodinuclear complexes using $(L^{2;2})^{2-}$ to $(L^{2;4})^{2-}$ have clarified the macrocyclic effect upon site selectivity for metal ions, providing heterodinuclear $M^{II}Cu^{II}$ and $Cu^{II}M^{II}$ core complexes.

References

1 O. Kahn, *Struct. Bonding* (*Berlin*), 1987, **68**, 89.
2 P. Zanello, S. Tamburini, P. A. Vigato and G. A. Mazzocchin, *Coord. Chem. Rev.*, 1987, **77**, 165.
3 P. A. Vigato, S. Tamburini and D. E. Fenton, *Coord. Chem. Rev.*, 1990, **106**, 25.
4 S. Gambarotta, F. Arena, C. Floriani and P. F. Zanazzi, *J. Am. Chem. Soc.*, 1982, **104**, 5082; F. Arena, C. Floriani, A. Chiesi-Villa and C. Guastini, *Inorg. Chem.*, 1986, **25**, 4589.
5 M. Sakamoto, M. Takagi, T. Ishimori and H. Ōkawa, *Bull. Chem. Soc. Jpn.*, 1988, **61**, 1613; M. Sakamoto, T. Ishimori and H. Ōkawa, *Bull. Chem. Soc. Jpn.*, 1988, **61**, 3319; Y. Aratake, H. Ōkawa, E. Asato, H. Sakiyama, M. Kodera, S. Kida and M. Sakamoto, *J. Chem. Soc., Dalton Trans.*, 1990, 2941.

6 M. Yamami, H. Furutachi, T. Yokoyama and H. Ōkawa, *Chem. Lett.*, 1998, 211; M. Yamami, H. Furutachi, T. Yokoyama and H. Ōkawa, *Inorg. Chem.*, 1998, **37**, 6832.

7 F. Keller and A. J. Rippert, *Helv. Chim. Acta*, 1999, **82**, 125.

8 D. E. Fenton and H. Ōkawa, *Chem. Ber./Recueil*, 1997, **130**, 433.

9 C. Fraser, L. Johnston, A. L. Rheingold, B. S. Haggerty, G. K. Williams, J. Whelan and B. Bosnich, *Inorg. Chem.*, 1992, **31**, 1835; C. Fraser, R. Ostrander, A. L. Rheingold, C. White and B. Bosnich, *Inorg. Chem.*, 1994, **33**, 324; C. Fraser and B. Bosnich, *Inorg. Chem.*, 1994, **33**, 338; D. G. McCollum, L. Hall, C. White, A. Ostrander, A. L. Rheingold, J. Whelan and B. Bosnich, *Inorg. Chem.*, 1994, **33**, 924; D. G. McCollum, C. Fraser, R. Ostrander, A. L. Rheingold and B. Bosnich, *Inorg. Chem.*, 1994, **33**, 2383; D. G. McCollum, G. P. A. Yap, A. L. Rheingold and B. Bosnich, *J. Am. Chem. Soc.*, 1996, **118**, 1365; D. G. McCollum, G. P. A. Yap, L. Liable-Sands, A. L. Rheingold and B. Bosnich, *Inorg. Chem.*, 1997, **36**, 2230.

10 S. Karunakaran and M. Kandaswamy, *J. Chem. Soc., Dalton Trans.*, 1994, 1595; S. Karunakaran and M. Kandaswamy, *J. Chem. Soc., Dalton Trans.*, 1994, 1595.

11 G. A. Melson, *Coordination Chemistry of Macrocyclic Compounds*, Plenum, New York, 1979.

12 M. Yonemura, Y. Matsumura, M. Ohba, H. Ōkawa and D. E. Fenton, *Chem. Lett.*, 1996, 601.

13 M. Yonemura, Y. Matsumura, H. Furutachi, H. Ōkawa and D. E. Fenton, *Inorg. Chem.*, 1997, **36**, 2711.

14 M. Yonemura, M. Ohba, K. Takahashi, H. Ōkawa and D. E. Fenton, *Inorg. Chim. Acta*, 1998, **283**, 72.

15 N. F. Curtis, *J. Chem. Soc.*, 1961, 3147.

16 E. A. Boudreaux and L. N. Mulay, *Theory and Applications of Molecular Paramagnetism*, Wiley, New York, 1976, pp. 491–496.

17 TEXSAN, Molecular Structure Analysis Package, Molecular Structure Corporation, Houston, TX, 1985 and 1992.

18 M. Yonemura, Y. Nakamura, N. Usuki and H. Ōkawa, *Chem. Commun.*, 2000, 817.

19 C. K. Johnson, ORTEP II, Report ORNL-5138, Oak Ridge National Laboratory, Oak Ridge, TN, 1976.

20 J. Ferguson, *J. Chem. Phys.*, 1961, **34**, 2206.

21 S. J. Gruber, C. M. Harris and E. Sinn, *J. Inorg. Nucl. Chem.*, 1968, **30**, 1805.

22 B. Xiong, B. Song, J. Zuo, X. You and X. Huang, *Polyhedron*, 1995, **15**, 903.

23 B. Bosnich, *J. Am. Chem. Soc.*, 1968, **90**, 627.

24 R. S. Downing and F. L. Urbach, *J. Am. Chem. Soc.*, 1969, **91**, 5977.

25 W. J. Geary, *Coord. Chem. Rev.*, 1971, **7**, 81.

26 A. W. Addison, T. N. Rao, J. Reedijk, J. V. Rijn and G. C. Verschoor, *J. Chem. Soc., Dalton Trans.*, 1984, 1349.

27 C. C. Chao, *J. Magn. Reson.*, 1973, **10**, 1.

28 R. P. Scaringe, D. J. Hodgson and W. E. Hatfield, *Mol. Phys.*, 1978, **35**, 701.

29 B. Bleaney and K. D. Bowers, *Proc. R. Soc. London, Ser. A*, 1952, **214**, 451.

30 A. G. Manfredotti and C. Guastini, *Acta Crystallogr., Sect. C*, 1983, **39**, 863.

31 R. H. Holm, *J. Am. Chem. Soc.*, 1960, **82**, 5632.

32 W. C. Hoyt and G. W. Everett, Jr., *Inorg. Chem.*, 1969, **8**, 2013.

33 A. T. Casey and S. Mitra, *Theory and Applications of Molecular Paramagnetism*, eds. E. A. Boudreaux and L. N. Mulay, Wiley, New York, 1976, pp. 220–226.